Patterns in small aspect ratio Bénard-Marangoni convection

M. L. Ramón, D. Maza, and H. L. Mancini

Departamento de Física y Matemática Aplicada, Facultad de Ciencias, Universidad de Navarra, 31080 Pamplona, Navarra, Spain

(Received 23 December 1998)

An experimental study of pattern formation in Bénard-Marangoni convection with small aspect ratio containers and high Prandtl number fluids is presented. The observed stationary patterns complete previous experimental works performed at different values of aspect ratio and supercriticality. Detailed experimental studies of the flow in some single structures are described, and spatial bifurcations between different stationary planforms for a fixed aspect ratio are shown. These experimental results agree qualitatively with linear theory analysis and with some previous numerical works about boundary conditions effects.
[S1063-651X(99)18910-4]

PACS number(s): 47.54.+r, 47.20.Dr, 47.27.Te

I. INTRODUCTION

Since the experiment of Bénard in 1900 [1], it is well-known that when a fluid layer is heated from below, the fluid begins to move, yielding a cellular pattern as soon as the temperature difference between the top and the bottom overcomes a critical value ΔT_c. When the upper surface is open to the atmosphere (like in Bénard's experiments), two mechanisms are responsible for convective motions: the variation of the fluid density with temperature (*buoyancy effect*) and the variation of the surface tension with temperature (*thermocapillary effect*). Their contribution can be measured by means of two adimensional numbers: the Rayleigh number $\mathrm{Ra} = \alpha g d^3 \Delta T / \kappa \nu$ (α = thermal expansion coefficient, g = gravity, d = fluid depth, κ = thermal diffusivity, ν = kinematic viscosity), and the Marangoni number $\mathrm{Ma} = g d \Delta T |\sigma'| / \kappa \eta$ ($|\sigma'|$ = variation with temperature of the surface tension coefficient, η = dynamic viscosity). The systems wherein these two forces are present at once are known as Bénard-Marangoni convection (BMC). They are related, respectively, to buoyancy and surface tension. When the convective movement begins, two dissipative mechanisms tend to stop it: lateral heat diffusion and viscosity [1]. As a general feature, the convective flow is self-organized in cells with lateral dimensions similar to the layer depth [2].

In the last decades, experiments on BMC have been performed mostly in enclosures with horizontal dimensions D much larger than the fluid layer depth d, i.e., in *large aspect ratio* systems (LAR). In these LAR systems, the influence of the lateral wall symmetries is negligible. The patterns are composed of a large number of hexagonal cells characterized by the presence of defects, each of them formed by irregular hexagonal cells or by polygonal cells with a different number of sides.

The only geometric dimension suitable for the scaling is the layer depth d. When D becomes comparable to d, only a few cells fit the container size and the effects of the lateral walls can not be ignored. Symmetry imposes restrictions on the resulting patterns and affects strongly the instability thresholds. Under these circumstances, the problem is known as *small aspect ratio* convection (SAR) [3–5].

Several questions emerge when dealing with SAR systems. Concerning the geometry, what kind of pattern (or cell structure) appears near threshold for a given aspect ratio Γ? In particular, the role of symmetries in the pattern shape and the dynamics of the arising structure need to be investigated. Only a few experimental works in BMC are available if compared with theoretical works. Even though experiments and theory agree qualitatively (for example, in the fact that the number of appearing cells increases with the aspect ratio), there are also some points of disagreement.

Koschmieder and Prahl [5] have shown experimentally the influence of the lateral walls on the pattern selection in SAR enclosures containing high Prandtl number fluids. By using cylindrical and square lateral walls, they have observed a sequence of patterns that exhibits an increasing number of azimuthal nodal lines as Γ increases. Their experimental results partially confirmed theoretical studies carried out previously by Rosenblat *et al.* [3,4], despite the fact that only one driving force (surface tension) was considered in the theory. As Koschmieder and Prahl remark, there are general coincidences and also several discrepancies between the results of [5] and [3,4]. For cylindrical containers, theory and experiment differ in the sequence of the modes as a function of Γ. One of the discrepancies is the first convective state that must appear in the lowest Γ region. Furthermore, in the simplest patterns, the SAR enclosures display very similar features for different proportions between destabilizing forces and different Γ [consider, e.g., Figs. 1(c), 3(a), and 3(b) of [5]]. This suggests that the aspect ratio is not the only relevant geometrical parameter; the depth must be considered separately, since the buoyancy indicator (Ra) grows with d^3 and the corresponding one for the surface tension (Ma) linearly with d. Thus, an increment of d reinforces in a stronger way the buoyancy contribution to convection.

Ondarçuhu *et al.* [6] reported the experimental ordering of the azimuthal structures (denoted in [6] as single modes), together with several new patterns with *radial* divisions and one or more hexagons at larger Γ values. Furthermore, Ref. [6] shows evidence of different spatial bifurcations between two stationary states taking place as the heating is increased beyond the convective threshold.

The analytical model of Rosenblat *et al.* considered adiabatic impenetrable slippery walls and negligible surface de-
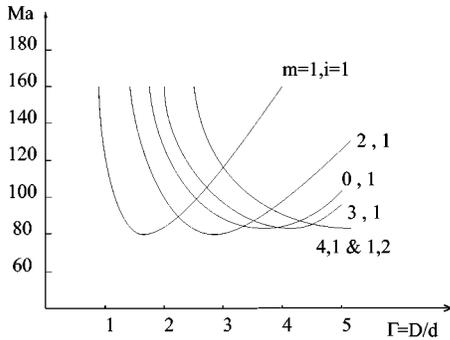
FIG. 1. Marginal stability curve as a function of the aspect ratio Γ, reconstructed from Fig. 1 of Rosenblat *et al.* [3]. m and i stand for azimuthal and radial wavelength respectively.

FIG. 2. Outline of the experimental setup. See the work of Ondarçuhu *et al.* [11] for details.

flections. By a linear analysis, they obtained the marginal stability curve as a function of Γ, i.e., the critical Marangoni number Ma_c for the different convective states, concretely at Rayleigh number Ra=0 (see Fig. 1). Besides, they showed separately the dependence of this curve versus Ra and Biot number (Bi), a nondimensional indicator of the heat transfer from the fluid to air in the free surface.

After Rosenblat *et al.*, other theoretical and numerical works have regarded the boundary influence on the patterns and on the ordering of modes when both driving forces are considered, in BMC with cylindrical symmetry [7–9]. Since SAR implies (comparatively) large d, it is clear that buoyancy cannot be neglected on the earth's surface. Echebarria *et al.* [7] paid attention to a resonant interaction near a codimension-2 point in cylindrical containers (previously studied in [3]), but now including thermocapillary and gravitational effects, and considered not only the amplitude of the unstable modes but also their phase dynamics.

Three-dimensional systems have been studied numerically (see references in [8,9] for a detailed list of these works). Zaman and Narayanan [8] studied a linear convection problem considering thermocapillary and gravitational effects, including more realistic lateral boundary conditions. They determined the patterns that appear in cylindrical geometry near the onset of convection for different values of Γ, showing that the axisymmetrical solution (a toroidal roll) is stable for a large range of Γ. Dauby *et al.* [9] proposed a different numerical analysis of a similar linear model, in order to study the dependence of Ma_c on Γ, considering Ra and Bi numbers as parameters. They checked that the sequence of patterns observed as Γ increases near threshold was different in the cases of perfect conducting or insulating lateral walls.

In contrast with Rayleigh-Bénard convection, or BMC with large aspect ratio, works in BMC with small Γ are scarce. In cylindrical geometry, only a small number of experiments have shown reproducible results in time dependent BMC (rotating and oscillating structures, traveling waves, etc.) [10–14].

In this paper we report experimental results obtained in SAR cylindrical containers near the convective instability threshold. We have focused our experimental study on stationary states, discussing the ordering of the structures when Γ is modified. In Sec. II the experimental techniques are briefly described. Experimental results are shown in Sec. III
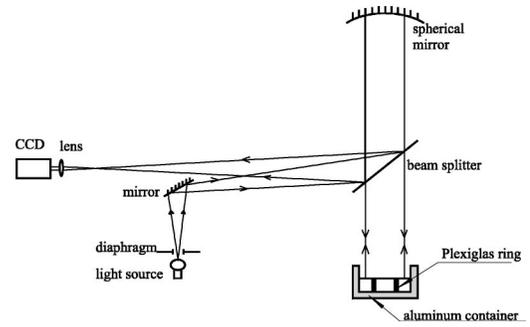
and then discussed. Finally, the most relevant conclusions are drawn.

II. EXPERIMENTAL SETUP

The experimental setup is sketched in Fig. 2. A cylindrical aluminum container is heated from below by an electrical resistance stuck to the bottom of the container (a 13-mm-thick disk). A regulated power supply keeps the level of heating constant at a preset value. In our experiments, we have place cylindrical rings of Plexiglas inside the cell in order to change Γ. All the rings have the same thickness and cover the height range from 7.5 mm to 24.9 mm (Γ from 1.4 to 10.5). Their thermal properties are similar to those of the silicon oil.

The fluid used in our experiments is a 350 centi Stokes silicon oil (99.5% purity), whose physical properties change less than 5% over all the temperature range of the experiment. Its Prandtl number (Pr=3097) is large enough to consider the thermal diffusion time as a characteristic time of the experience (Pr=τ_{th}/τ_v, where $\tau_{th}=l^2/\kappa$ is the characteristic thermal diffusion time, and $\tau_v=l^2/\nu$ the viscous diffusion time, with l=typical length of the system). In order to estimate τ_{th} in the horizontal (vertical) direction, we have chosen the radius (fluid depth) as a typical length. In the following, the notation used is τ_{th}^h (τ_{th}^v).

The container is filled to a level such that the liquid reaches the rim of the internal ring. In this way, the surface of the fluid is almost flat, minimizing the meniscus effects. We have verified that rigid insulating walls surrounded by the same fluid and at the same mean temperature avoid the formation of horizontal gradients of temperature. The depth of the fluid layer is measured with an error smaller than 10 μm.

Temperature measurements are performed by means of small thermocouples (diameter=0.5 mm), and infrared sensors when a noninvasive measure is needed. A data acquisition system is used to obtain temperature data files, and a parallel beam shadowgraph system allows the simultaneous observation of the planform (see Fig. 2).

A detailed explanation of the shadowgraph setup can be found in [6]. In our case, the surface of the heater was not polished, in order to diffuse the incoming light. Consequently, the optical system provides only information about surface deflections.

In all our experiment, the fluid moves along the surface

from the *raised* hot regions to the *depressed* cold ones. As a result, the thin bright lines correspond to zones where the surface deformation, acts as a convergent mirror. Moreover, in these zones the fluid goes down, i.e., the largest velocity component is in the negative z direction (from up to down).

This method turns out to be inappropriate for detecting patterns near the onset of convection, since the small surface deflections do not provide noticeable intensity variations. We have made use of alternative detecting methods, namely: (a) Tracer particles (aluminum powder, with a mean size of 20 μm) are used to highlight the streamlines on the free surface. Once deposited on this surface, the particles (visible by the scattering of white light) float and follow the fluid motion. Streak photography of their movement provides images of the fluid trajectories on the surface. (b) The motion in the bulk of the fluid can be detected by depositing colored silicon oil drops inside the fluid. Due to the long diffusion time of the colorant, whole three-dimensional (3D) streamlines remain marked. These last two techniques provide excellent results for comparing experimental results with predictions made in theoretical and numerical studies [3,7,9,13].

III. EXPERIMENTAL RESULTS

First of all, we present the convective structures observed for increasing values of Γ. We increase the heating power very slowly for each Γ until a pattern can be detected. Convective structures are compared with the critical modes (m,i) reported by Rosenblat *et al.* [3], where m and i stand for the azimuthal and radial wave numbers (see Fig. 1).

For the smallest values of Γ, a structure consisting of one warm point near the lateral wall can be observed. From this point, the fluid tends to approach the diametrically opposed zone of the cell. This structure is not visible by shadowgraphy. Figure 3(a) shows an image obtained by streak photography of tracer particles for $\Gamma = 1.8$ and $\Delta T = 7.1\,°C$. Flow departs from the warm point near the wall, forming streak lines only slightly curved, recalling a shell. In order to draw information about the motion in the bulk, colored silicon oil drops have been deposited in the middle of the free surface. For this initial position and the same experimental conditions, we have found the streamlines shown in Fig. 3(c).

Figures 3(b) and 3(d) present the simulation of fluid motion on the surface and in the bulk for the mode (1,1) of Fig. 1, obtained following the theoretical linear analysis of [3]. There is a clear relationship between mode (1,1) and the experimental images [Figs. 3(a) and 3(c)]. In the discussion, we will compare them in a greater detail.

For $\Gamma = 2.1$ and $\Delta T = 7.1\,°C$, two hot points can coexist close to the wall on opposite sides of the cell. By means of shadowgraphy, a cold line is seen separating them [Fig. 4(a)]. For the same parameter values, the streak lines shown in Fig. 4(b) have been obtained. They can be contrasted to mode (2,1) presented in Fig. 4(c). The two warm points are the sources of the streamlines, which form curved trajectories ending at the surface in the cold line of the structure.

The streamlines resulting from the deposition of colored silicon oil drops in the cold points of the free surface are presented in Fig. 4(d). These streamlines tend to remain inside a quadrant (defined by the cold segment and the diam-
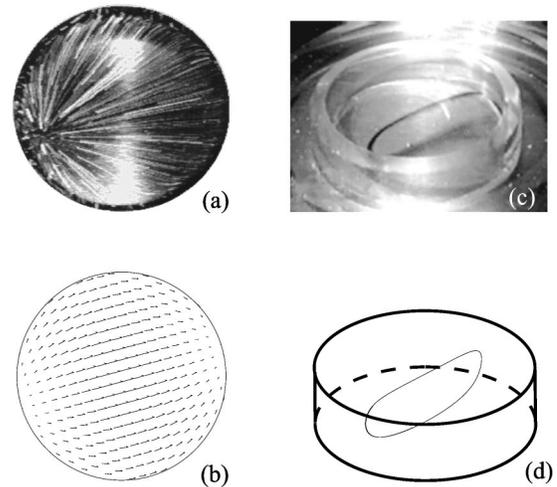

FIG. 3. Pattern observed for $\Gamma = 1.8$ ($D = 44.5$ mm, $d = 24.9$ mm) and $\Delta T = 7.1\,°C$ (Ra/Ma=97, Ma=280). (a) Streak photography of the motion on the free surface, provided by aluminum particles deposited on it. Flow departs in nearly all directions from a hot point near the lateral wall. Streak lines are slightly curved to the diametrically opposed point of the cell. (b) Numerical simulation of surface motion for the critical mode (1,1) of [3]. (c) Experimental streamlines in the bulk: path followed by silicon colored oil. The streamline shown goes around a whole diametrical section of the cell. (d) Numerical simulation of the motion in the bulk for the critical mode (1,1) of [3]. One streamline going around a diametrical section is found again.

eter perpendicular to it). The characteristic flow velocity for this and the previous structure is about 1 cm/min, measured by image particle velocimetry [15]. In order to compare Fig. 4(d) with theoretical predictions, we enclose the simulation of fluid motion for the mode (2,1) [Fig. 4(e)].

This pattern can be induced by a suitable metal sheet on the free surface, but it loses stability in a time of the order of $17\tau_{th}^{h}$ (or $18\tau_{th}^{v}$) in the most favorable cases. We have checked this feature by inducing this structure for values of Γ between 1.8 and 2.3. After this interval of time, the ''cold segment'' gives rise to one of its neighboring structures on the marginal stability curve (see Fig. 1). The asymmetry of Fig. 4(b) is related to the difficulty of stabilizing this highly symmetrical structure in real experimental conditions.

For slightly greater values of Γ, we found a new structure with one warm region placed in the center of the cell: fluid rises by the center and falls near the sidewall. This completely symmetrical pattern consisting of one circular roll has been observed close to the threshold for $\Gamma = 2.36$, 2.75, 3.75, and 3.95. In a shadowgraph, the warmer area of the center can be distinguished [see Fig. 5(b), where $\Gamma = 3.95$ and $\Delta T = 14.2\,C$].

Increasing the values of Γ, a sequence of structures consisting of azimuthal partitions (like pieces of a cake) has been obtained. A pair of such structures is shown in Fig. 5, together with the ''cold line'' and the symmetrical structure. The number of partitions increases with ΔT and Γ.

From $\Gamma \approx 6$, a radial division appears just at the onset of convection. Figure 6(a) shows a structure consisting of two circular concentric rolls. Fluid rises by the center and near the sidewall of the cell, and falls by the bright circumference
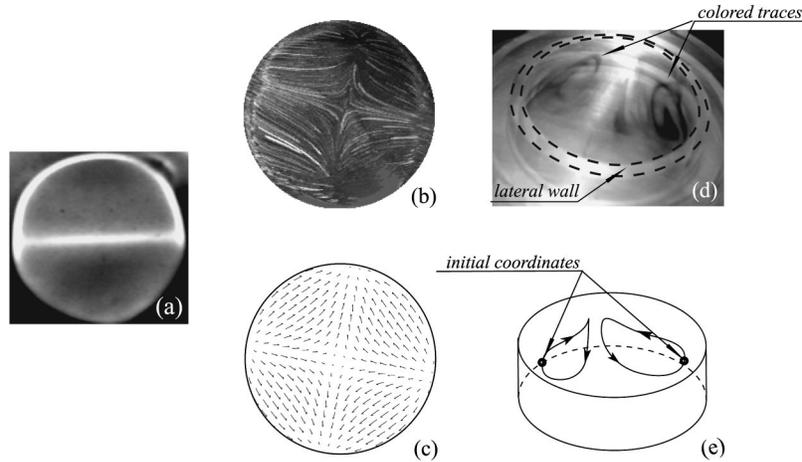
FIG. 4. Pattern observed for $\Gamma=2.1$ ($D=52.2$ mm, $d=25.2$ mm) and $\Delta T=7.1\,°C$ (Ra/Ma=94, Ma=279). (a) Shadowgraph of the pattern. The central bright line corresponds to the zone where fluid goes down (the bright semicircumference is due to a spurious reflection on the lateral wall). (b) Streak photography of the free surface: fluid rises by two warm points near the sidewall and falls near a diameter of the cell (the cold line of the structure). The real experimental conditions make difficult the observation of a perfect symmetrical pattern. (c) Numerical simulation of surface motion for the critical mode (2,1) of [3]. It can be compared to (b). (d) Streamlines in the bulk. Colored drops of silicon oil have been injected in the center of the fluid. The two nearly closed streamlines tend to remain inside the quadrants defined by the cold line of the structure and the diameter perpendicular to it. (e) Numerical simulation of the motion of ''two colored drops'' in the bulk for the critical mode (2,1) of Rosenblat *et al.* The initial conditions of the simulation and the experiment are practically the same. There is a clear relationship between this traces and the previous ones.

shown in the image forming two toroidal rolls. Nevertheless, for slightly greater power values the radial division can be replaced again by the azimuthal structures. The same kinds of azimuthal divisions have been found added to the radial one [see Figs. 6(b), 6(c), and 6(d), where the flow rises by the center of the lobes and near the lateral wall, and falls along the white lines of the shadowgraph]. The structure shown in Fig. 6(d) has been obtained by induction (for $\Gamma = 10.5$ and $\Delta T = 22.5\,°C$) and has remained observable for a time of the order of $5.6\tau_{th}^{h}$ ($158.5\tau_{th}^{V}$).

An ordered sequence of the structures found for increasing values of Γ is shown in Figs. 7(a) and 7(b). They are represented in (a) by a simulation of free-surface streamlines and in (b) by an outline of their shadowgraph images. As can be checked in Fig. 7(b), symmetrical patterns are not the only ones observed: we found an asymmetrical structure for $\Gamma = 5.2$ and $\Delta T = 12.8\,°C$.

From $\Gamma \approx 8$, a pattern consisting of one hexagon can be found when the heating is increased (near the onset but not

as a primary instability). The number of hexagons appearing in the structure increases with Γ, giving rise to the hexagonal pattern first observed by Bénard in large aspect ratio systems. In LAR it is well established that the wavelength of periodic patterns is approximately twice the layer depth. Analogously, in SAR systems for certain structures (like the hexagonal one) an *equivalent wavelength* satisfying this ratio can be defined.

IV. DISCUSSION OF THE RESULTS

We have obtained an experimental verification of the ordering of modes predicted by the linear theory [3] for small values of Γ. For the smallest Γ, the first structure observed consists of flow moving from a small region near the wall to the diametrically opposed area. The hypothetical boundary conditions of the linear analysis performed by Rosenblat
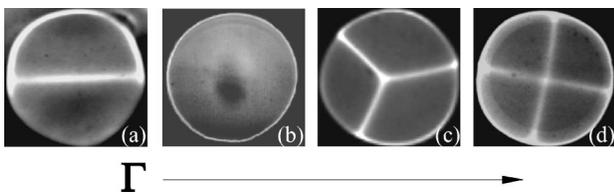

FIG. 5. Shadowgraph images obtained for different structures under the following conditions: (a) the ''white segment,'' for $\Gamma=2.1$, $\Delta T=7.1\,°C$ (Ra/Ma=94, Ma=279); (b) ''one circular roll,'' for $\Gamma=3.95$, $\Delta T=14.2\,°C$ (Ra/Ma=38, Ma=360); (c) three nodal divisions for $\Gamma=6.3$, $\Delta T=11.4\,°C$ (Ra/Ma=15, Ma=180); (d) four nodal divisions for $\Gamma=7.45$, $\Delta T=11.15\,°C$ (Ra/Ma=15, Ma=176). The bright lines mark the zones where fluid goes down.
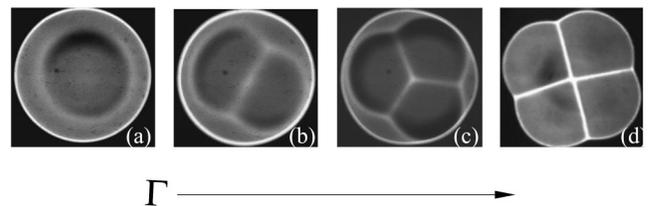

FIG. 6. Shadowgraph images obtained for structures with radial and azimuthal divisions. It can be contrasted with Fig. 5. Bright lines show the cold zones (where fluid falls). Fluid goes up near the lateral walls and inside the lobes formed by the bright lines. (a) ''Two concentric rolls:'' $\Gamma=8.75$, $\Delta T=10.65\,°C$ (Ra/Ma=10.6, Ma=143). (b) ''Two lobes:'' $\Gamma=9.5$, $\Delta T=11.9\,°C$ (Ra/Ma=9, Ma=147.5). (c) ''Three lobes:'' $\Gamma=10$, $\Delta T=14.9\,°C$ (Ra/Ma=8, Ma=175.5). (d) ''Four lobes:'' $\Gamma=10.5$, $\Delta T=22.5\,°C$ (Ra/Ma=18, Ma=397).
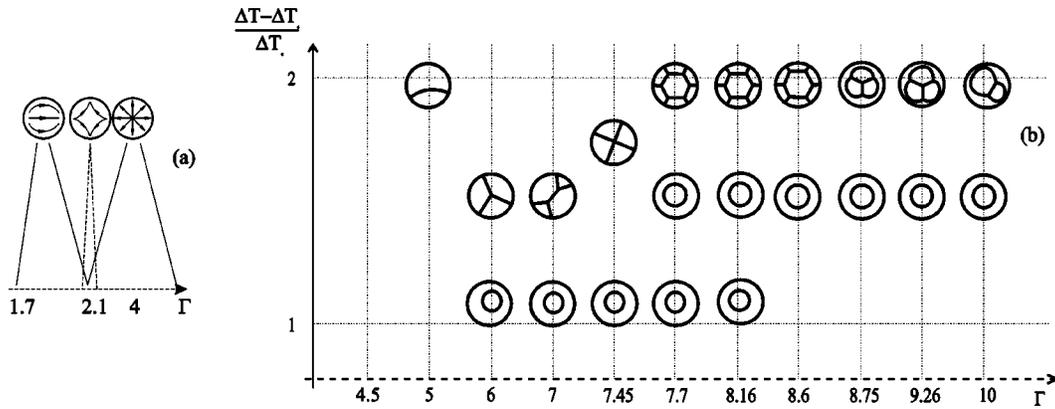
FIG. 7. Outline of most of the structures experimentally observed in SAR systems for arbitrarily distributed values of Γ. (a) The three principal structures observed for $\Gamma \lesssim 4$. They are represented by a simulation of the streamlines on the free surface. The second one is a structure that is difficult to stabilize. (b) The vertical axis is an estimation of the *supercriticality* for the patterns' appearance [$\epsilon = (\Delta T - \Delta T_c)/\Delta T_c$, where ΔT_c is the minimum temperature difference for which convection has been observed]. Radial divisions appear from $\Gamma \approx 5$, and the hexagonal structure (typical in BMC) from $\Gamma \approx 8$. As in LAR systems, polygonal structures are formed from the previous radial division of the system for larger values of ϵ.

et al. [3] led to streamlines going up and down touching the lateral wall. However, for realistic lateral conditions, the nonslip boundary conditions at the walls prevent the fluid from moving near them. This difference is not the only discrepancy between Figs. 3(a) and 3(b): the curvature of streak lines in the simulation is hardly noticeable in our image. The combined effects of surface deflections, realistic lateral walls, and the unavoidable meniscus may cause the differences observed, which could also be explained as the result of a combination of the critical modes (1,1) and (2,1) giving rise to a ''mixed mode'' [7]. The streamlines obtained by means of colorant tracers described nearly closed trajectories between opposite sides of the cell [Fig. 3(c)]. This structure is in agreement with the mode (1,1) solved numerically by Dauby *et al.* introducing realistic boundary conditions [9] (warning: mode nomenclature changes in [9]).

When Γ is slightly increased, according to Rosenblat *et al.* the subsequent critical mode expected consists of fluid going up by two diametrically opposed points near the wall, as has been obtained experimentally [see the streak lines of Fig. 4(b)]. We have observed that the warm point of the previous pattern can remain near the wall, allowing the presence of a new warm point near the opposite side of the wall and giving rise to the ''white segment'' pattern. It is difficult to attain the experimental conditions necessary to preserve such a highly symmetrical structure. Small thermal fluctuations or other kinds of perturbations can lead to a symmetry breaking: one of the warm points is reinforced and consequently ''moves the white line towards the wall,'' causing the other warm point to disappear. The remaining warm region can move towards the center, forming the toroidal pattern. In Fig. 4(b), the slight lack of symmetry that finally leads to the disappearance of the bright line can be observed. In spite of its short ''life,'' in our opinion this pattern does not represent a transient state: we have verified that it can be present for more than $10 \, \tau_{th}$.

The observed loss of stability of this structure is in line with the stability curve obtained numerically in [9], where the structure is masked by the circular roll mode. We have observed the ''white segment'' pattern [Fig. 4(a)] for a value

of Γ similar to the one predicted by linear theory [3]; however, this value is smaller than those reported by Koschmieder and Prahl [5] ($\Gamma = 5.31$) and Ondarçuhu *et al.* [6] ($\Gamma = 4.5$). The next critical modes (3,1), (4,1) and (1,2) of Fig. 1 correspond to the patterns of Fig. 5(c) and Fig. 5(d), the asymmetrical structure found for $\Gamma = 5.2$, respectively. For greater values of Γ, the pattern described as a ''circular roll'' or as a ''toroidal flow pattern'' is present just at the threshold in all the works performed in SAR systems with cylindrical geometry.

With regard to the differences found between linear theory and experimental observations, Zaman and Narayanan [8] justify them by bunching modes predicted for aspect ratio values near 3 (they suggest that it is preferable to work with smaller or with larger aspect ratios). More recently, these discrepancies were also pointed out by Dauby *et al.* [9]. They concluded that a linear analysis of the structures does not provide a good description of the experimentally observed patterns.

Another interesting result is the appearance of the modes with radial divisions and an increasing number of azimuthal nodal lines shown in Fig. 6. There is a clear distinction between the situation in which the horizontal diameter of the container is smaller than the *equivalent wavelength* and when instead it is larger. For the minor values of D, the structures consist of divisions like pieces of a cake, in a number that increases with Γ and the distance over threshold. Only when D admits a circular roll, can the first hexagon appear. Structures similar to those of Fig. 6 have been reported in the numerical work of Dauby *et al.* [9]. However, some differences exist in the order in which these structures appear (as a function of Γ) and also in the value of the aspect ratio where these modes destabilize.

Finally, Echebarria *et al.* have predicted a time dependent regime between the aforementioned modes (1,1) and (2,1). In their work [7], they proved for Ra/Ma$\lesssim$20 that the stability region of the heteroclinic orbit enlarges when Ra/Ma decreases. In our experiment, Ra/Ma$\gtrsim$20; the persistence of the stability region in this case should be checked. We ob-

serve neither this regime nor the one observed by Johnson and Narayanan [13] between modes (0,1) and (2,1) (there is a nomenclature change again).

V. CONCLUSIONS

We have verified experimentally that the ordering of modes corresponds to that predicted by linear theory [3] for small Γ values. Temporal regimes between different structures in the lowest aspect ratios have not been observed. Increasing Γ, structures consisting of azimuthal divisions, radial divisions, or a combination of them appear. Hexagonal patterns can be observed from $\Gamma \approx 8$ for sufficiently large power values (not just at the onset).

[1] H. Bénard, Rev. Gen. Sci. Pures Appl. **11**, 1261 (1900); **11**, 1309 (1900).

[2] *Cellular Structures in Instabilities*, edited by J.E. Wesfreid and S. Zalesky (Springer-Verlag, Berlin, 1984).

[3] S. Rosenblat, S. H. Davis, and G. M. Homsy, J. Fluid Mech. **120**, 91 (1982).

[4] S. Rosenblat, G. M. Homsy, and S. H. Davis, J. Fluid Mech. **120**, 123 (1982).

[5] E. L. Koschmieder and S. A. Prahl, J. Fluid Mech. **215**, 571 (1990).

[6] T. Ondarçuhu, J. Millán-Rodríguez, H. L. Mancini, A. Garcimartín, and C. Pérez-García, Phys. Rev. E **48**, 1051 (1993).

[7] B. Echebarria, D. Krmpotiĉ, and C. Pérez-García, Physica D **99**, 487 (1997).

[8] A. A. Zaman and R. Narayanan, J. Colloid Interface Sci. **179**, 151 (1996).

[9] P. C. Dauby, G. Lebon, and E. Bouhy, Phys. Rev. E **56**, 520 (1997).

[10] T. Ondarçuhu, G. Mindlin, H. L. Mancini, and C. Pérez-García, Phys. Rev. Lett. **70**, 3892 (1993).

[11] T. Ondarçuhu, G. Mindlin, H. L. Mancini, and C. Pérez-García, J. Phys.: Condens. Matter **6**, A427 (1994).

[12] H. L. Mancini, doctoral thesis, Universidad de Navarra, Spain 1994 (unpublished).

[13] D. Johnson and R. Narayanan, J. Colloid Interface Sci. **54**, R3102 (1996).

[14] H. L. Mancini and D. Maza, Phys. Rev. E **55**, 2757 (1997).

[15] W. Merzkirsch, *Flow Visualization*, 2nd ed. (Academic Press, Orlando, 1987).